

Vacuum-enhanced optical nonlinearities with disordered molecular photoswitchesMarina Litinskaya^{1,*} and Felipe Herrera^{2,3,†}¹*Department of Physics & Astronomy and Department of Chemistry, University of British Columbia, Vancouver, Canada V6T 1Z1*²*Department of Physics, Universidad de Santiago de Chile, Avenida Ecuador 3493, Santiago, Chile*³*Millennium Institute for Research in Optics (MIRO), Concepción, Chile*

(Received 10 April 2018; revised manuscript received 11 December 2018; published 10 January 2019)

It is well known that nonlinear optical signals such as cross-phase modulation can be coherently enhanced in multilevel atomic gases under conditions of electromagnetically induced transparency, but analogous results in solids are challenging to obtain due to natural energetic disorder. We propose a solid-state cavity QED scheme to enable cross-phase modulation between two arbitrarily weak classical fields in the optical domain, using a highly disordered intracavity medium composed of organic molecular photoswitches. Even in the presence of strong energetic and orientational disorder, the unique spectral properties of organic photoswitches can be used to enhance the desired nonlinearity under conditions of vacuum-induced transparency, enabling cross-phase modulation signals that surpass the detection limit imposed by absorption losses. Possible applications of the scheme include integrated all-optical switching with low photon numbers.

DOI: [10.1103/PhysRevB.99.041107](https://doi.org/10.1103/PhysRevB.99.041107)

The generation of nonlinear optical signals in solids requires the use of intense lasers because the nonlinear susceptibility of materials is small and difficult to manipulate. On the other hand, the optical response of atomic gases can be routinely manipulated via quantum interference effects such as coherent population trapping (CPT) [1] and electromagnetically induced transparency (EIT) [2], which has enabled the development of quantum memories [3] based on slow light [4], atomic clocks [5], and nonlinear optics at the level of individual photons [6]. In solids, coherent optical schemes analogous to those observed in atomic gases have been implemented with rare-earth doped crystals [7], quantum wells [8], and quantum dots [9] in samples with negligible inhomogeneous broadening at cryogenic temperatures. Attempts to implement coherent optical schemes with inhomogeneously broadened NV centers in diamond [10,11] have shown that unavoidable static energy fluctuations in the system severely restrict the quality of the quantum interference effects responsible for EIT. In atomic gases, it is always possible to suppress the detrimental effects of inhomogeneous broadening due to the Doppler shift of the transition frequencies involved, by adjusting the propagation direction, frequency, and intensity of the driving lasers [12]. However, no analogous mechanism is known for compensating static energy level fluctuations in the condensed phase.

In recent years, the demonstration of the strong and ultra-strong coupling regimes of cavity quantum electrodynamics (QED) at room temperature with organic molecular emitters in optical microcavities [13–17] has stimulated the development of integrated quantum technology that exploits quantum optics to enhance the natural transport and optical properties of organic materials [18–22]. However, efforts for

exploiting strong coupling in microcavities to establish CPT and EIT with molecular aggregates have failed because energy disorder unavoidably degrades the electronic interference necessary to establish coherent optical effects [23], even at cryogenic temperatures.

We develop a theory for a solid-state cavity QED scheme to implement vacuum-induced transparency (VIT) [24,25] as well as cross-phase modulation (XPM) between two arbitrarily weak coherent fields that interact with a strongly disordered medium composed of organic molecular photoswitches [26–28]. Achieving VIT is a prerequisite for coherence-based XPM with low photon numbers [29]. In this Rapid Communication, we extend the theory in Ref. [29], which is valid only for homogeneously broadened atomic gases, by taking into account the dominant role of inhomogeneous broadening due to static electronic energy disorder on all the molecular transitions involved. Our analysis is motivated by unique features in the electronic structure of organic photoswitches that are not present in other molecular species. We show that organic photoswitches can naturally support conditions for VIT in high-quality nanoscale optical cavities, despite strong energy disorder.

The envisioned light-matter scheme is shown in Fig. 1. The ground electronic potential of the photoswitch (S_0) has two deep wells in the isomerization coordinate corresponding to the *cis* and *trans* molecular isomers [26]. The lowest vibrational state of the *trans* isomer is the stable ground state of the system $|1\rangle$. The metastable ground state $|2\rangle$ corresponds to the lowest vibrational level of the *cis* isomer potential well. Thermal isomerization of state $|2\rangle$ is energetically forbidden at room temperature [26]. The lowest excited potentials S_1 and S_2 [30] correspond to states $|3\rangle$ and $|4\rangle$, respectively. The vibrational structure of the excited potentials is not resolved in condensed phase, but S_0 has spectrally resolved torsional modes with frequencies in the range $\omega_v \sim 160\text{--}190$ meV/ \hbar [31].

*litinskaya@gmail.com

†felipe.herrera.u@usach.cl

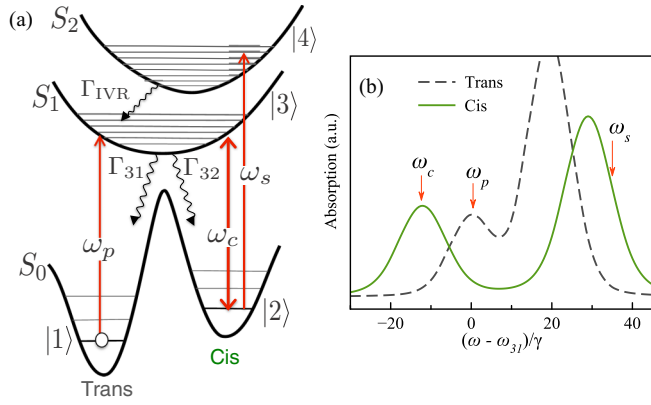


FIG. 1. Light-matter coupling scheme. (a) Level structure of molecular photoswitches. Straight arrows indicate near-resonant light-matter couplings at the cavity (ω_c), probe (ω_p), and signal (ω_s) frequencies. Curly arrows indicate nonradiative decay. (b) Absorption spectrum of the molecular photoswitch. The strongest *trans* band corresponds to the transition $S_0 \rightarrow S_2$.

Our model does not require an exact knowledge of the molecular potentials. Instead, we impose a set of constraints on the inhomogeneously broadened photoswitch absorption spectrum outside the cavity, which we illustrate in Fig. 1(b). The photoswitch spectrum should have (i) a well-resolved band associated with the *cis* transition $|2\rangle \rightarrow |3\rangle$, resonant with the cavity frequency ω_c , (ii) a well-resolved band associated with the *trans* transition $|1\rangle \rightarrow |3\rangle$, near resonant with the probe frequency $\omega_p > \omega_c$, and (iii) a well-resolved band associated with the *cis* transition $|2\rangle \rightarrow |4\rangle$, weakly driven by a blue-detuned signal field at frequency $\omega_s > \omega_p$. These spectral requirements can be met by *orthogonal* molecular photoswitches [32–34].

For a single emitter, the light-matter coupling scheme in Fig. 1 can be modeled by the Hamiltonian

$$\begin{aligned} \hat{H}_S = & \omega_c \hat{a}^\dagger \hat{a} + \omega_{21} |2\rangle \langle 2| + \omega_{31} |3\rangle \langle 3| + \omega_{41} |4\rangle \langle 4| \\ & + \Omega_c (|3\rangle \langle 2| \hat{a} + |2\rangle \langle 3| \hat{a}^\dagger) + \Omega_p (|3\rangle \langle 1| e^{-i\omega_p t} \\ & + |1\rangle \langle 3| e^{i\omega_p t}) + \Omega_s (|4\rangle \langle 2| e^{-i\omega_s t} + |2\rangle \langle 4| e^{i\omega_s t}), \quad (1) \end{aligned}$$

where Ω_p and Ω_s are the probe and signal semiclassical Rabi frequencies, respectively. Ω_c is the cavity vacuum Rabi frequency, and \hat{a} is the annihilation operator of the cavity field. In a dressed-state picture, our electronic basis must be supplemented with the cavity states to read $|\tilde{1}\rangle \equiv |1; 0_c\rangle$, $|\tilde{2}\rangle \equiv |2; 1_c\rangle$, $|\tilde{3}\rangle \equiv |3; 0_c\rangle$, and $|\tilde{4}\rangle \equiv |4; 1_c\rangle$. The probe field thus drives the transition $|\tilde{1}\rangle \leftrightarrow |\tilde{3}\rangle$, the signal field the transition $|\tilde{2}\rangle \leftrightarrow |\tilde{4}\rangle$, and the cavity field strongly admixes the nearly degenerate dressed states $|\tilde{2}\rangle$ and $|\tilde{3}\rangle$.

We model energy disorder in the Hamiltonian \hat{H}_S by defining the random transition frequencies $\omega_{31} = \langle \omega_{31} \rangle + \delta_{31}$, $\omega_{32} = \langle \omega_{32} \rangle + \delta_{32}$, and $\omega_{42} = \langle \omega_{42} \rangle + \delta_{42}$, where $\langle \omega_{ji} \rangle$ corresponds to the band center frequency and δ_{ji} is a random static fluctuation that gives rise to the inhomogeneous linewidths σ_{ji} . Linewidths due to energy disorder are typically in the range 150–200 meV for organic photoswitches [35], magnitudes that far exceed the typical homogeneous linewidth. In addition to energy disorder, below we also model orientational

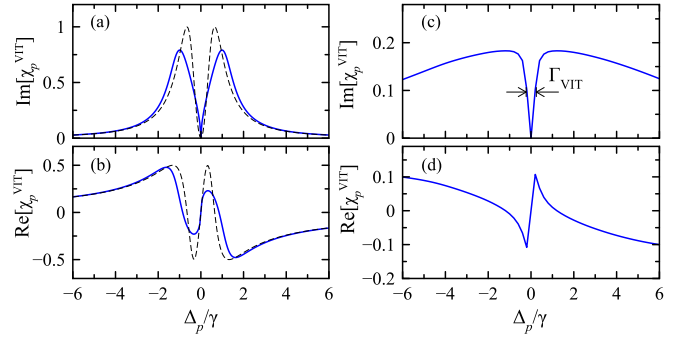


FIG. 2. Disorder-averaged absorptive ($\text{Im}\langle \chi_p^{\text{VIT}} \rangle$) and dispersive response ($\text{Re}\langle \chi_p^{\text{VIT}} \rangle$) of molecular photoswitches as a function of the probe detuning $\Delta_p = \omega_p - \langle \omega_{31} \rangle$, for a resonant cavity field $\omega_c = \langle \omega_{32} \rangle$. (a), (b) Uniform orientational disorder on the vacuum Rabi frequency with mean amplitude $\Omega_0 = 1.2\gamma$. For comparison, the dashed line shows the disorder-free VIT line shape. (c), (d) Gaussian disorder on ω_{31} for $\sigma = 6\gamma$ and $\Omega_c = 1.2\gamma$. The VIT linewidth Γ_{VIT} is also defined. In all panels we use $\gamma_{21} = 0.01\gamma$ and $\delta_{31} = \delta_{32}$. Frequency is given in units of the homogeneous linewidth γ .

disorder in the system by writing the vacuum Rabi frequency as $\Omega_c = \Omega_0 \cos \theta$, where Ω_0 is a constant amplitude and θ is a uniformly distributed random angle between the molecular transition dipole moment and the space-fixed cavity field polarization.

In general, the ultrafast dynamics of photoisomerization involves a complex interplay between nonadiabatic coupling and nonsecular relaxation [36]. Since we are only interested in the steady-state response of the cavity subject to continuous driving, we ignore the transient femtosecond dynamics of the system and adopt a coarse-grained Lindblad quantum master equation approach to describe dissipation. The bare photon lifetime is assumed in the range $1/\kappa \sim 10\text{--}100$ ps, which can be achieved using high- Q dielectric cavities [37]. Nonradiative decay of the excited state $S_2 \rightarrow S_1$ by intramolecular vibrational relaxation (IVR) has a lifetime $1/\Gamma_{\text{IVR}} \sim 0.1$ ps [38]. Nonradiative decay $S_1 \rightarrow S_0$ into the *trans* and *cis* ground states occurs at the rates Γ_{31} and Γ_{32} , respectively. The homogeneous probe absorption linewidth is defined as $\gamma = \Gamma_{31} + \Gamma_{32}$, with typical excited-state lifetimes in the range $1/\gamma \sim 0.1\text{--}0.5$ ps [35,39]. Finally, we account for pure dephasing of the coherence between the vibrational ground states $|1\rangle$ and $|2\rangle$ at the rate Γ_{pd} , with typical dephasing times in the range $1/\Gamma_{\text{pd}} \sim 1\text{--}100$ ps [40–43], depending on the molecular species, solvent, and temperature.

We derive an expression for the disorder-free susceptibility of the organic medium at the probe frequency χ_p , as described in Sec. S1 of the Supplemental Material (SM) [44]. We then obtain the disorder-averaged susceptibility $\langle \chi_p \rangle$ by analytically integrating over random dipole orientations θ and over the random frequency shifts δ_{ij} . The results are used to describe the photophysics of inhomogeneously broadened molecular photoswitches in nanoscale optical cavities.

We begin by assuming that no signal field is present ($\Omega_s = 0$). In Fig. 2, we show the corresponding disorder-averaged susceptibility $\langle \chi_p^{\text{VIT}} \rangle$ as a function of the mean probe detuning $\Delta_p = \omega_p - \langle \omega_{31} \rangle$, for the representative decay ratios

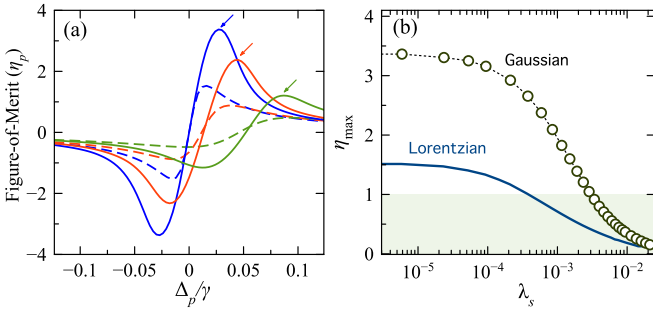


FIG. 3. XPM figure of merit (η_p) for different signal parameters λ_s . (a) $\langle \eta_p \rangle$ vs probe detuning Δ_p for $\lambda_s = 0$ (blue line), $\lambda_s = 0.5$ (red), and $\lambda_s = 1$ (green). Solid and dashed lines correspond to Gaussian and Lorentzian disorder, respectively. Arrows indicate the optimal figure of merit. (b) $\langle \eta_{\max} \rangle$ as a function of λ_s for Gaussian ($\sigma = 5\gamma$) and Lorentzian disorder with equal width (FWHM). The shaded region corresponds to signal-to-noise ratios below unity. We use $\gamma_{21} = 2 \times 10^{-3}\gamma$ and $\Omega_c = 0.8\gamma$ in both panels.

$\Gamma_{\text{pd}}/\gamma = 10^{-2}$ and $\kappa/\gamma = 10^{-4}$. We numerically average the homogeneous response over a large number of disorder configurations. For the orientational average, Figs. 2(a) and 2(b) confirm that random dipole orientations do not significantly alter the coherent optical properties of organic cavities [45]. The analytical average in Eq. (S16) of the SM coincides exactly with the numerical average.

We numerically average energy disorder by taking random frequency fluctuations δ_{ji} from independent Gaussian distributions with the same standard deviation, i.e., $\sigma_{ji} = \sigma$. Figures 2(c) and 2(d) show the characteristic signatures of VIT despite inhomogeneous broadening due to energy disorder ($\sigma = 6\gamma$): strong suppression of the probe absorption (transparency) and steep dispersion (slow light), over a narrow frequency window around the two-photon resonance condition $\Delta_p - \Delta_c = 0$ [2], with $\Delta_c \equiv \omega_c - \langle \omega_{32} \rangle$ being the cavity detuning. The survival of VIT in the presence of disorder can be understood analytically by averaging $\langle \chi_p^{\text{VIT}} \rangle$ using a Lorentzian disorder model, as discussed in Sec. S2-B of the SM. The Lorentzian model is found to underestimate the quality of VIT in comparison with a more realistic Gaussian disorder, as Fig. 3(b) below shows. Within the Lorentzian model, the homogeneous linewidth γ_{ij} associated with transition $|i\rangle \leftrightarrow |j\rangle$ is simply replaced by $\Sigma_{ij} = \gamma_{ij} + \sigma_{ij}$, i.e., the inhomogeneous linewidth is just an additive contribution to the total linewidth. This result also holds for XPM, as discussed below. For a disorder-free system (e.g., atomic gases), a high-visibility VIT signal would require that $\gamma_{21} \ll \Omega_c \leq \gamma$ [24]. As long as disorder only affects the probe transition $|\tilde{1}\rangle \rightarrow |3\rangle$, we can rewrite these conditions as follows,

$$\gamma_{21} \ll \Omega_c \leq \Sigma_{31}, \quad (2)$$

where $\gamma_{21} \equiv \kappa/2 + \Gamma_{\text{pd}}$ is the decay rate of the coherence between dressed states $|\tilde{1}\rangle$ and $|\tilde{2}\rangle$, and $\Sigma_{31} \equiv (\gamma/2 + \sigma_{31})$ is the total probe *trans* absorption linewidth, with σ_{31} being the static energy fluctuations of states $|\tilde{1}\rangle$ and $|\tilde{2}\rangle$ are equal, i.e., $\delta_{31} = \delta_{32}$. The quality of VIT degrades as we allow the two ground isomer potential minima to fluctuate independently,

setting a constraint on the contribution of inhomogeneous broadening on the vibrational Raman frequency ω_{21} to be much smaller than the excited-state linewidth γ . If ω_{21} were to fluctuate significantly, the intracavity Raman dark state $|D\rangle = \sqrt{a}|\tilde{1}\rangle + \sqrt{1-a}|\tilde{2}\rangle$ ($0 < a < 1$) [2] would rapidly dephase, breaking the CPT effect that causes the VIT.

In molecular photoswitches, both *cis* and *trans* isomers belong to the same molecular orbital. Therefore, we expect that $|\delta_{31} - \delta_{32}|/\gamma \ll 1$ in a condensed-phase environment, enabling conditions for VIT. This would not be the case if the vibrational ground states $|1\rangle$ and $|2\rangle$ belong to different molecular orbitals, highlighting the unique features of organic photoswitches over other molecular species for the implementation of coherent optics in condensed phase.

Having established the physical conditions for achieving VIT with disordered molecular photoswitches, we now discuss the desired XPM scheme involving simultaneous driving of the intracavity medium with both probe and signal fields. We focus on the phase shift Φ experienced by the probe field due to copropagation with a signal field over a given path length. Attenuation at the probe frequency is quantified by the absorption coefficient α . Under conditions of VIT, both Φ and α not only depend on the probe and signal field frequencies and Rabi frequencies, but also on the cavity vacuum parameters [24,46]. Following Ref. [47], we define the figure of merit $\langle \eta_p \rangle = \text{Re}\langle \chi_p \rangle / 2 \text{Im}\langle \chi_p \rangle$ to quantify the degree by which it is possible to interferometrically resolve the XPM phase shift Φ at frequency ω_p . Detectable nonlinear signals require $\langle \eta_p \rangle > 1$.

In Sec. S3 of SM, we develop an analytical approximation for the disorder-averaged susceptibility $\langle \chi_p \rangle$ in the presence of both probe and signal fields. We integrate the disorder-free susceptibility over the random fluctuations (δ_{31} , δ_{42}) assuming that they belong to independent Lorentzian distributions with different widths. Lorentzian averaging compares well with Gaussian disorder for $\Omega_s = 0$ [12,48], and is analytically tractable for the analysis of cross-phase modulation signals. We derive an expression for $\langle \chi_p \rangle$ in Eq. (S19) in SM, from which we can write the mean figure of merit

$$\langle \eta_p(x) \rangle = \frac{1}{2} \frac{\Omega_c^2(x - x_s) - x A_s(x)}{\Sigma_{31} A_s(x) + \Omega_c^2(\gamma_{21} + \gamma_s)}, \quad (3)$$

where $x \equiv \Delta_p$ is the probe detuning. The function $A_s(x) \equiv (x - x_s)^2 + (\gamma_{21} + \gamma_s)^2$ is given in terms of the frequency shift $x_s \equiv \lambda_s \Delta_s$ and width $\gamma_s \equiv \lambda_s \Sigma_{41}$, with all the signal properties are combined into the parameter

$$\lambda_s \equiv \Omega_s^2 / (\Delta_s^2 + \Sigma_{41}^2), \quad (4)$$

where $\Delta_s = \omega_s - \langle \omega_{42} \rangle$ is the mean signal detuning and $\Sigma_{41} \equiv \kappa/2 + \Gamma_{\text{IVR}}/2 + \sigma_{42}$, where σ_{42} is the inhomogeneous linewidth of the *cis* absorption band. In Sec. S4-B of the SM, we show that λ_s exclusively captures the effect of the signal field on $\langle \chi_p \rangle$.

Outside the cavity ($\Omega_c = 0$), Eq. (3) simply reduces to the linear response result $\langle \eta_p \rangle = -\Delta_p / 2 \Sigma_{31}$, which near resonance gives $\langle \eta_p \rangle \ll 1$ due to absorption of the probe field. In the presence of the cavity vacuum, but without signal driving ($\Omega_s = 0$), the figure of merit $\langle \eta_p(\Omega_s = 0) \rangle \equiv \langle \eta_{\text{VIT}} \rangle$ can be considered as a degree of coherence in the response of the

medium to the probe field. In this VIT regime, Eq. (3) reduces to Eq. (S21) of the SM, which can be written as

$$\langle \eta_{\text{VIT}}(x) \rangle \approx \frac{\Omega_c^2 x}{2(\Sigma_{31} x^2 + \gamma_{21} \Omega_c^2)} \gg 1, \quad (5)$$

when $\gamma_{21} \ll x \ll \Omega_c$.

For a system dominated by inhomogeneous broadening ($\gamma \ll \sigma_{31}$) and a long-lived dressed vibrational coherence ($\gamma_{21} \ll \gamma$), Eq. (5) has a maximum at the probe detuning $x_* = \Omega_c \sqrt{\gamma_{21}/\sigma_{31}}$ that is blueshifted from the VIT absorption minimum, giving the optimal figure of merit

$$\langle \eta_{\text{VIT}}^{\text{max}} \rangle = \Omega_c / \sqrt{16 \gamma_{21} \sigma_{31}}. \quad (6)$$

We next discuss the behavior of Eq. (3) under simultaneous probe and signal driving ($\Omega_s > 0$), when the figure of merit is directly related to the magnitude of the XPM signal [47]. Coupling to the signal field tends to destroy VIT, by weakly admixing the dark state $|D\rangle$ (see above) with the fast-decaying excited dressed state $|\tilde{4}\rangle$. The maximum achievable figure of merit $\langle \eta_{\text{max}} \rangle$ subject to signal driving therefore cannot exceed the VIT maximum in Eq. (6), i.e., $\langle \eta_{\text{max}} \rangle \leq \langle \eta_{\text{VIT}}^{\text{max}} \rangle$ for any λ_s , with the equality sign holding only when $\lambda_s = 0$.

We can use Eq. (3) to find the constraints on x_s and γ_s that allow the nonlinear figure of merit to approach the VIT limit $\langle \eta_{\text{VIT}}^{\text{max}} \rangle$. For instance, in realistic organic systems dominated by inhomogeneous broadening with $\Sigma_{41} \approx \Sigma_{31} \approx \sigma$ and assuming $\Omega_c/|\Delta_s| \leq \sqrt{\gamma_{21}/\sigma}$, our Lorentzian disorder model predicts that it is possible to reach $\langle \eta_{\text{max}} \rangle \gtrsim 1$ under a single constraint on the dimensionless signal parameter, given by $\lambda_s \lesssim \gamma_{21}/\sigma \ll 1$. In summary, large values of $\langle \eta_{\text{max}} \rangle$ can be reached by the following: (i) decreasing Ω_s , as the signal field partly destroys VIT, as it is not protected by the transparency window; (ii) increasing Δ_s , making the incoherent signal field less resonant and therefore less absorptive; and (iii) increasing σ_{41} , effectively distributing the signal beam among many frequencies, many of which are far-detuned from $\langle \omega_{24} \rangle$ and therefore less absorptive.

We finally compare the predictions of our Lorentzian disorder model [Eq. (3)] with a Gaussian model, which is more experimentally relevant. Figure 3(a) shows the $\eta(x)$ profiles predicted by the Lorentzian model and the result of numerical integration with δ_{31} and δ_{42} taken from independent Gaussian distributions, again assuming $\delta_{31} = \delta_{32}$ as in Fig. 2.

We find that even when the Gaussian and Lorentzian noise distributions have equal widths [full width at half maximum (FWHM)], Gaussian disorder consistently allows for higher values of $\langle \eta_{\text{max}} \rangle$. This behavior is captured in Fig. 3(b), which shows that for fixed γ_{21} and Ω_c , the XPM signal in systems with Gaussian absorption are detectable for values of λ_s that are nearly an order of magnitude higher than those predicted by the Lorentzian model, reducing the experimental constraints on the signal field. Figure 3(b) also shows that the Lorentzian model underestimates the asymptotic VIT bound on $\langle \eta_{\text{max}} \rangle$ as $\lambda_s \rightarrow 0$.

By studying the dependence of the desired XPM signal on the dephasing rate γ_{21} , we find that the scaling of the upper bound $\langle \eta_{\text{VIT}}^{\text{max}} \rangle \sim \Omega_c / \sqrt{\gamma_{21}}$ predicted by the Lorentzian model [Eq. (6)] can also accurately describe the behavior of the upper bound for Gaussian disorder (see Fig. S3 of SM). In other words, a larger vacuum Rabi frequency Ω_c can compensate for a large dephasing rate γ_{21} , in order to achieve detectable XPM signals.

In summary, we propose an organic cavity QED scheme to achieve large cross-phase modulation signals using *arbitrarily weak* probe and signal fields, despite strong energetic and orientational disorder in the material. The scheme exploits a long-lived vibrational coherence between the *cis* and *trans* ground vibrational states in a class of chromophores known as molecular photoswitches, to establish conditions for VIT. In addition to conventional high- Q microcavities, the proposed scheme could be implemented with an ensemble of N nanoscale optical cavities, each containing a single molecular photoswitch with random dipole orientation and electronic energy gaps, within the cavity mode volume. Ensembles of single-emitter nanoscale organic cavities can be prepared and optically probed using nanophotonic techniques [49–51]. Our results thus pave the way for the development of organic-based integrated nanophotonic devices for all-optical switching at ultralow power levels.

We thank Stéphane Kéna-Cohen for comments. M.L. thanks Universidad de Santiago de Chile for hospitality during early stages of this work. F.H. is supported by Iniciativa Científica Milenio (ICM) through the Millennium Institute for Research in Optics (MIRO), and by CONICYT through the Proyecto REDES ETAPA INICIAL, Convocatoria 2017 No. REDI 170423, and FONDECYT Regular No. 1181743.

-
- [1] H. R. Gray, R. M. Whitley, and C. R. Stroud, Coherent trapping of atomic populations, *Opt. Lett.* **3**, 218 (1978).
- [2] M. Fleischhauer, A. Imamoglu, and J. P. Marangos, Electromagnetically induced transparency: Optics in coherent media, *Rev. Mod. Phys.* **77**, 633 (2005).
- [3] M. Fleischhauer and M. D. Lukin, Quantum memory for photons: Dark-state polaritons, *Phys. Rev. A* **65**, 022314 (2002).
- [4] L. V. Hau, S. E. Harris, Z. Dutton, and C. H. Behroozi, Light speed reduction to 17 metres per second in an ultracold atomic gas, *Nature (London)* **397**, 594 (1999).
- [5] J. Vanier, Atomic clocks based on coherent population trapping: A review, *Appl. Phys. B* **81**, 421 (2005).
- [6] T. Peyronel, O. Firstenberg, Q.-Y. Liang, S. Hofferberth, A. V. Gorshkov, T. Pohl, M. D. Lukin, and V. Vuletić, Quantum nonlinear optics with single photons enabled by strongly interacting atoms, *Nature (London)* **488**, 57 (2012).
- [7] B. S. Ham, P. R. Hemmer, and M. S. Shahriar, Efficient electromagnetically induced transparency in a rare-earth doped crystal, *Opt. Commun.* **144**, 227 (1997).
- [8] M. C. Phillips, H. Wang, I. Rumyantsev, N. H. Kwong, R. Takayama, and R. Binder, Electromagnetically Induced Transparency in Semiconductors Via Biexciton Coherence, *Phys. Rev. Lett.* **91**, 183602 (2003).

- [9] X. Xu, B. Sun, P. R. Berman, D. G. Steel, A. S. Bracker, D. Gammon, and L. J. Sham, Coherent population trapping of an electron spin in a single negatively charged quantum dot, *Nat. Phys.* **4**, 692 (2008).
- [10] P. R. Hemmer, A. V. Turukhin, M. S. Shahrar, and J. A. Musser, Raman-excited spin coherences in nitrogen-vacancy color centers in diamond, *Opt. Lett.* **26**, 361 (2001).
- [11] V. M. Acosta, K. Jensen, C. Santori, D. Budker, and R. G. Beausoleil, Electromagnetically Induced Transparency in a Diamond Spin Ensemble Enables All-Optical Electromagnetic Field Sensing, *Phys. Rev. Lett.* **110**, 213605 (2013).
- [12] J. Gea-Banacloche, Y.-Q. Li, S.-Z. Jin, and M. Xiao, Electromagnetically induced transparency in ladder-type inhomogeneously broadened media: Theory and experiment, *Phys. Rev. A* **51**, 576 (1995).
- [13] D. G. Lidzey, D. D. C. Bradley, M. S. Skolnick, T. Virgili, S. Walker, and D. M. Whittaker, Strong exciton-photon coupling in an organic semiconductor microcavity, *Nature (London)* **395**, 53 (1998).
- [14] T. W. Ebbesen, Hybrid light-matter states in a molecular and material science perspective, *Acc. Chem. Res.* **49**, 2403 (2016).
- [15] S. Kéna-Cohen, S. A. Maier, and D. D. C. Bradley, Ultrastrongly coupled exciton-polaritons in metal-clad organic semiconductor microcavities, *Adv. Opt. Mater.* **1**, 827 (2013).
- [16] F. Herrera and F. C. Spano, Absorption and photoluminescence in organic cavity QED, *Phys. Rev. A* **95**, 053867 (2017).
- [17] F. Herrera and F. C. Spano, Theory of nanoscale organic cavities: The essential role of vibration-photon dressed states, *ACS Photonics* **5**, 65 (2018).
- [18] J. A. Hutchison *et al.*, Modifying chemical landscapes by coupling to vacuum fields, *Angew. Chem., Int. Ed. Engl.* **51**, 1592 (2012).
- [19] E. Orgiu *et al.*, Conductivity in organic semiconductors hybridized with the vacuum field, *Nat. Mater.* **14**, 1123 (2015).
- [20] G. Lerario, A. Fieramosca, F. Barachati, D. Ballarini, K. S. Daskalakis, L. Dominici, M. D. Giorgi, S. A. Maier, G. Gigli, and S. Kéna-Cohen, Room-temperature superfluidity in a polariton condensate, *Nat. Phys.* **13**, 837 (2017).
- [21] B. Liu, M. J. Crescimanno, and K. D. Singer, Linear and nonlinear optical properties of organic cavity polaritons in the ultrastrong regime, in *Frontiers in Optics 2017*, OSA Technical Digest (online) (Optical Society of America, Washington, D.C., 2017), paper JTU3A.51.
- [22] F. Barachati, J. Simon, Y. A. Getmanenko, S. Barlow, S. R. Marder, and S. Kéna-Cohen, Tunable third-harmonic generation from polaritons in the ultrastrong coupling regime, *ACS Photonics* **5**, 119 (2018).
- [23] F. Herrera *et al.*, Quantum nonlinear optics with polar J-aggregates in microcavities, *J. Phys. Chem. Lett.* **5**, 3708 (2014).
- [24] J. E. Field, Vacuum-Rabi-splitting-induced transparency, *Phys. Rev. A* **47**, 5064 (1993).
- [25] H. Tanji-Suzuki, W. Chen, R. Landig, J. Simon, and V. Vuletić, Vacuum-induced transparency, *Science* **333**, 1266 (2011).
- [26] C. Dugave and L. Demange, Cis-trans isomerization of organic molecules and biomolecules: Implications and applications, *Chem. Rev.* **103**, 2475 (2003).
- [27] S. Kawata and Y. Kawata, Three-dimensional optical data storage using photochromic materials, *Chem. Rev.* **100**, 1777 (2000).
- [28] R. S. Stoll and S. Hecht, Artificial light-gated catalyst systems, *Angew. Chem., Int. Ed. Engl.* **49**, 5054 (2010).
- [29] H. Schmidt and A. Imamoglu, Giant Kerr nonlinearities obtained by electromagnetically induced transparency, *Opt. Lett.* **21**, 1936 (1996).
- [30] H. M. Dhammika Bandara and S. C. Burdette, Photoisomerization in different classes of azobenzene, *Chem. Soc. Rev.* **41**, 1809 (2012).
- [31] N. Biswas, B. Abraham, and S. Umapathy, Investigation of short-time isomerization dynamics in *p*-nitroazobenzene from resonance Raman intensity analysis, *J. Phys. Chem. A* **106**, 9397 (2002).
- [32] D. Bléger, J. Schwarz, A. M. Brouwer, and S. Hecht, *o*-fluoroazobenzenes as readily synthesized photoswitches offering nearly quantitative two-way isomerization with visible light, *J. Am. Chem. Soc.* **134**, 20597 (2012).
- [33] C. E. Weston, R. D. Richardson, P. R. Haycock, A. J. P. White, and M. J. Fuchter, Arylazopyrazoles: Azoheteroarene photoswitches offering quantitative isomerization and long thermal half-lives, *J. Am. Chem. Soc.* **136**, 11878 (2014).
- [34] M. M. Lerch, M. J. Hansen, W. A. Velema, W. Szymanski, and B. L. Feringa, Orthogonal photoswitching in a multifunctional molecular system, *Nat. Commun.* **7**, 12054 (2016).
- [35] C. M. Stuart, R. R. Frontiera, and R. A. Mathies, Excited-state structure and dynamics of *cis*- and *trans*-azobenzene from resonance Raman intensity analysis, *J. Phys. Chem. A* **111**, 12072 (2007).
- [36] F. Rodriguez-Hernandez, A. Martinez-Mesa, and L. Uranga-Pina, Hybrid quantum-classical study of the non-adiabatic *cis-trans* photoisomerization in a model polyatomic molecule, *Chem. Phys. Lett.* **592**, 18 (2014).
- [37] L. Collot, V. Lefèvre-Seguín, M. Brune, J. M. Raimond, and S. Haroche, Very high-*Q* whispering-gallery mode resonances observed on fused silica microspheres, *Europhys. Lett.* **23**, 327 (1993).
- [38] P. Hamm, S. M. Ohline, and W. Zinth, Vibrational cooling after ultrafast photoisomerization of azobenzene measured by femtosecond infrared spectroscopy, *J. Chem. Phys.* **106**, 519 (1997).
- [39] T. Fujino, S. Yu. Arzhantsev, and T. Tahara, Femtosecond time-resolved fluorescence study of photoisomerization of *trans*-azobenzene, *J. Phys. Chem. A* **105**, 8123 (2001).
- [40] K. Iwata, R. Ozawa, and H.-O. Hamaguchi, Analysis of the solvent- and temperature-dependent Raman spectral changes of *S*₁*trans*-stilbene and the mechanism of the trans to cis isomerization: A dynamic polarization model of vibrational dephasing and the C=C double-bond rotation, *J. Phys. Chem. A* **106**, 3614 (2002).
- [41] Q. H. Xu and M. D. Fayer, Temperature-dependent vibrational dephasing: Comparison of liquid and glassy solvents using frequency-selected vibrational echoes, *J. Chem. Phys.* **117**, 2732 (2002).
- [42] A. C. Terentis, L. Ujj, H. Abramczyk, and G. H. Atkinson, Primary events in the bacteriorhodopsin photocycle: Torsional vibrational dephasing in the first excited electronic state, *Chem. Phys.* **313**, 51 (2005).

- [43] M. Fujiwara, K. Yamauchi, M. Sugisaki, A. Gall, B. Robert, R. J. Cogdell, and H. Hashimoto, Energy dissipation in the ground-state vibrational manifolds of β -carotene homologues: A sub-20-fs time-resolved transient grating spectroscopic study, *Phys. Rev. B* **77**, 205118 (2008).
- [44] See Supplemental Material at <http://link.aps.org/supplemental/10.1103/PhysRevB.99.041107> for details on the theoretical framework, the derivation of all equations in the main text and further discussion about the role of two-photon dephasing rate on the XPM signal.
- [45] M. Litinskaya and P. Reineker, Loss of coherence of exciton polaritons in inhomogeneous organic microcavities, *Phys. Rev. B* **74**, 165320 (2006).
- [46] P. R. Rice and R. J. Brecha, Cavity induced transparency, *Opt. Commun.* **126**, 230 (1996).
- [47] H. Kang and Y. Zhu, Observation of Large Kerr Nonlinearity at Low Light Intensities, *Phys. Rev. Lett.* **91**, 093601 (2003).
- [48] A. Javan, O. Kocharovskaya, H. Lee, and M. Scully, Narrowing of electromagnetically induced transparency resonance in a Doppler-broadened medium, *Phys. Rev. A* **66**, 013805 (2002).
- [49] F. Benz, M. K. Schmidt, A. Dreismann, R. Chikkaraddy, Y. Zhang, A. Demetriadou, C. Carnegie, H. Ohadi, B. D. Nijs, R. Esteban, J. Aizpurua, and J. J. Baumberg, Single-molecule optomechanics in picocavities, *Science* **354**, 726 (2016).
- [50] R. Chikkaraddy, B. De Nijs, F. Benz, S. J. Barrow, O. A. Scherman, E. Rosta, A. Demetriadou, P. Fox, O. Hess, and J. J. Baumberg, Single-molecule strong coupling at room temperature in plasmonic nanocavities, *Nature (London)* **535**, 127 (2016).
- [51] R. Chikkaraddy, V. A. Turek, N. Kongsuwan, F. Benz, C. Carnegie, T. Van De Goor, B. de Nijs, A. Demetriadou, O. Hess, U. F. Keyser, and J. J. Baumberg, Mapping nanoscale hotspots with single-molecule emitters assembled into plasmonic nanocavities using DNA origami, *Nano Lett.* **18**, 405 (2018).